Three-dimensional imaging with axially distributed sensing using electronically controlled liquid crystal lens

Chih-Wei Chen,[1,†] Myungjin Cho,[2,†] Yi-Pai Huang,[1] and Bahram Javidi[3,*]

[1]*Department of Photonics & Institute of Electro-Optical Engineering, Display Institute, National Chiao Tung University, Hsinchu 30010, Taiwan*

[2]*Electrical, Electronic, and Control Engineering, Hankyong National University, Ansung, 456-749, South Korea*

[3]*Electrical and Computer Engineering Department, University of Connecticut, Storrs, Connecticut 06269, USA*

**Corresponding author: bahram@engr.uconn.edu*

Received July 19, 2012; accepted August 9, 2012;
posted August 20, 2012 (Doc. ID 172960); published September 28, 2012

In this Letter, we present a three-dimensional (3D) imaging system with axially distributed sensing (ADS) using an electronically controlled liquid crystal (LC) lens. The proposed system performed an optical image acquisition by varying the focal lengths of the LC lens without mechanical movements of an image sensor. Multiple images with slightly different perspectives were experimentally recorded, and the 3D images were reconstructed according to the ray backprojection algorithm. To the best of our knowledge, this is the first report on 3D ADS using a LC lens. The proposed system is attractive for compact 3D sensing camera systems.

OCIS codes: 110.6880, 230.3720.

Three-dimensional (3D) integral imaging has been used for 3D sensing and visualization. In an integral imaging system, a lens or camera array (laterally distributed) is used to capture 3D information from the scene, which is constructed by multiple two-dimensional (2D) images with different perspectives. 3D images can be reconstructed numerically or optically [1–6]. Axially distributed sensing (ADS) [7–8] has been proposed to record 3D data from the scene by moving a single image sensor along its optical axis. However, the mechanical movement of the image sensor in ADS may be impractical for a compact 3D image sensing system. Consequently, a system with nonmechanical movement is required. We propose to use the tunable liquid crystal (LC) lens [9–13] whose focal length can be electronically controlled. Varying the focal length electronically, multiple 2D images with slightly different perspectives can be obtained. In this Letter, we propose a 3D image sensing system that combines the ADS technique with the LC lens. Therefore, the axially distributed images can be obtained without mechanical movement of a sensor. Finally, experimental results of computational 3D reconstruction show that our proposed method is suitable to be implemented for a compact 3D image sensing system.

ADS is used to capture multiple 2D images with slightly different magnifications and perspectives of a 3D scene. The object is located at a certain distance away from the closest camera position. In conventional ADS, the camera moves along its optical axis and takes a number of 2D images. The object in the multiple 2D images will have different magnifications because each image is captured at a different distance from the object. Finally, 3D images can be reconstructed by the ray back propagation method [7,8].

For the LC lens, its refractive index distribution can be changed when applying a voltage onto the LC cell. Thus, the incident polarized light is supposed to be focused when the refractive index profile is a parabolic curve as follows [11]:

$$f_{\mathrm{LC}} = \frac{\rho^2}{2(n(\rho) - n_{\max})d}, \tag{1}$$

$$n(\rho) = \frac{1}{z}\int_0^z n(\rho, z)\mathrm{d}z, \tag{2}$$

where f is the focal length, d is the cell thickness, and ρ is the radial distance from optical axis. The $n_{\max}$ and $n(\rho)$ represent the refractive index on the optical axis, and the refractive index which drops off radially from $n_{\max}$ on the optical axis, respectively. The index $n(\rho)$ can be calculated by integrating every arbitrarily position, $\rho = (x^2 + y^2)^{1/2}$, along the z direction in the LC lens, as Eq. (2). Therefore, in this Letter, an exciting device, a high-resistance liquid crystal (HR-LC) lens [14–16], is utilized to obtain a parabolic profile LC lens. A high-resistance material (we use IGZO semiconductor material) is coated on the controlled electrodes layer, as shown in Fig. 1. Using the high-resistance layer, the gradient changed potential distribution can be easily produced when applying the different voltages between the center electrode, planar electrode, and edge electrode (see Fig. 1) Thus, the LC molecules will reorient according to the electric field. Finally, the parabolic curve of

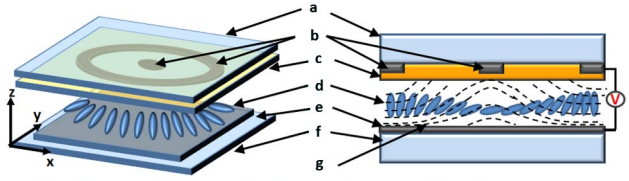

Fig. 1. (Color online) Structure of high-resistance liquid crystal (HR-LC) lens. High-resistance layer is coated on the controlled electrode layer.

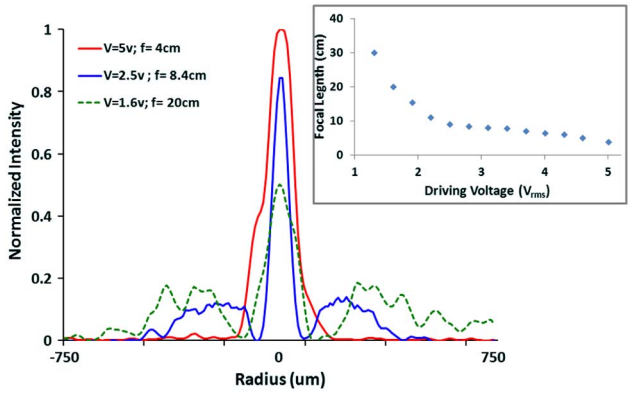

Fig. 2. (Color online) Experiments of light intensity distributions after passing through HR-LC lens for different driving voltages, and relationship between focal length and driving voltage.

$n(\rho)$ can be approached. In this Letter, we used an HR-LC lens whose diameter and LC cell gap are designed as 2 mm and 60 μm, respectively. The LC material is E7 (Merck) and it is aligned with the x direction. The polarized light is also aligned with the x direction. Finally, the focal length can be varied between 4 cm to ∞ when switching driving voltages from 5 V_{rms} to 0 V_{rms} (1 KHz frequency, square waveform). To verify the functionality of the HR-LC lens, a light source and a CCD located at the focal plane are used to measure the intensity distribution, as shown in Fig. 2. The measured results show that the tunable HR-LC lens with variable focal lengths under different driving voltages is really established, yet the focusing ability for each focal length still has variation. Through further analyzing, it is caused by the high-resistance layer, which is not perfectly optimized for every focal length. Thus, optimization of the HR-LC lens can be the next step. Fortunately, this issue does not affect our result, though some blurred images appear.

The proposed ADS system with HR-LC lens is shown in Fig. 3. The object is located in front of the LC lens and away from the optical axis. A CCD sensor is fixed and placed a distance (d) away from the LC lens. Changing the focal lengths, multiple 2D images with different magnifications (perspectives) can be captured (Fig. 3). For instance, the magnification factor M_j between the first image (the image taken by shortest focal length) and jth image (Fig. 3) can be described by Eq. (3):

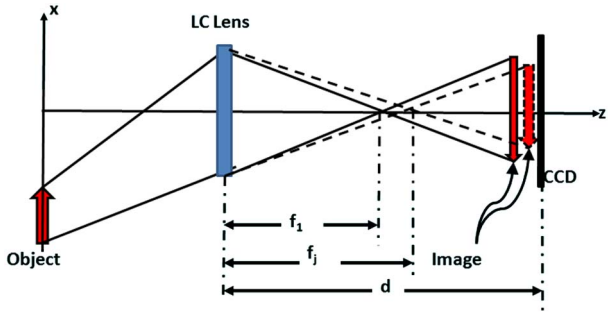

Fig. 3. (Color online) Setup of the proposed 3D sensing system: ADS using HR-LC lens.

$$M_j = \frac{f_1(d - f_j)}{f_j(d - f_1)}. \tag{3}$$

Following, the 3D images can be reconstructed by using these multiple 2D images and the ray backprojection algorithm. According to the ray backprojection algorithm, all 2D images are projected with different magnification factors on the reconstruction plane at z_r. Then the reconstructed 3D image $I(x, y, z_r)$ can be obtained by superimposing all the projected images with different magnification factors as the following:

$$I(x, y, z_r) = \frac{1}{K}\sum_{j=0}^{K-1} E_j\left(\frac{x}{M_{j\times(\frac{z_r}{z_0})}}, \frac{y}{M_{j\times(\frac{z_r}{z_0})}}, z_r\right), \tag{4}$$

where M_j is the corresponding magnification factor between the selected jth elemental image and the first elemental image as described in Eq. (3), E_j is the magnified jth elemental image, and K is the total numbers of recorded 2D images.

The preliminary functionality of the proposed 3D axially distributed image sensing system is demonstrated by optical experiments. The experimental setup is illustrated in Fig. 4. A slogan (words) and a totem are located at approximately 18 and 13 mm in front of the LC lens, respectively. A cell phone camera with 5 megapixels is used and fixed behind the LC lens to capture all in-focus 2D images. For the capturing process, the driving voltage of the LC lens is swept from 5 to 0 V_{rms} (~0.3 V/step) so that the focal length changed from 4 cm to ∞. Hence, the total $K = 14$ 2D images can be recorded sequentially.

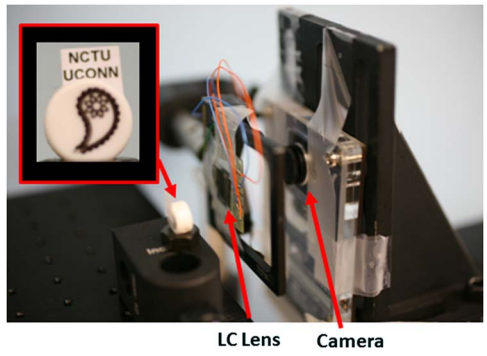

Fig. 4. (Color online) Experimental setup of ADS with HR-LC lens. The objects: slogan and totem are separated by 5 mm.

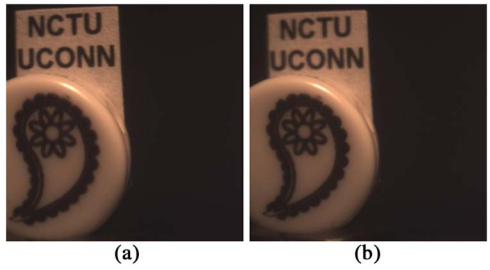

Fig. 5. (Color online) Examples of the recorded 2D elemental images with different focal lengths of HR-LC lens. (a) The first elemental image ($f_{LC} = 4$ cm) and (b) the twelfth elemental image ($f_{LC} = 20$ cm).

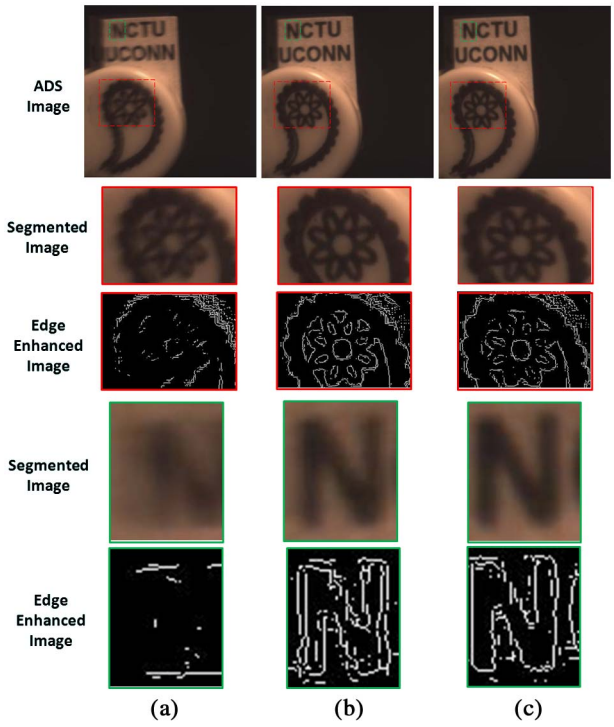

Fig. 6. (Color online) ADS experimental results. 3D computational reconstructions of the scene with different distances: (a) $z = 9$ mm, (b) $z = 13$ mm, and (c) $z = 18$ mm (part of the slogan and totem are selected to see more detail). The Sobel edge detector is used.

Figure 5 shows examples of the captured 1st and 12th 2D elemental images. We can distinguish the slight difference (magnification of the object) between the two images. Using computational reconstruction and all 2D recorded images, a 3D image can be reconstructed. Figure 6 shows the reconstruction results at $z = 9$ mm, $z = 13$ mm, and $z = 18$ mm away from the LC lens. The magnified areas are also chosen to illustrate more detail. In addition, in order to directly distinguish the differences between the results, the Sobel edge enhanced method [17] is also used. Therefore, the focused objects will produce the clear edge contour, as shown in Fig. 6. For the reconstructed image at $z = 9$ mm, both the slogan and totem are blurred. Especially, the slogan is blurrier than the totem because the slogan is farther away from the reconstruction plane [see Fig. 6(a)]. The totem can be observed clearly in the reconstructed image at $z = 13$ mm, yet the slogan is still blurred [see Fig. 6(b)]. On the other hand, the slogan is clear in the reconstructed image at $z = 18$ mm, nevertheless, the totem comes out blurred [see Fig. 6(c)]. Though we had demonstrated the functionality of the proposed method, the working range for this system is still limited by the NA of the HR-LC lens now. Therefore, developing the HR-LC lens with high-quality and larger NA, and using the computational distortion calibration method [18] to extend the working range for the proposed system could be the next step.

In conclusion, we have presented a novel 3D imaging system without mechanical movement by combining the ADS with an electronically controlled LC lens. Different focal lengths of the proposed HR-LC lens are also demonstrated. Finally, the reconstructed 3D images can be successfully generated from the recorded 2D images. The proposed system is attractive for compact 3D sensing camera applications.

The authors acknowledge the support by the National Science Council, Taiwan, under projects NSC101-2917-I-009-006 and No. NSC101-2221-E-009-120-MY3. We also would like to thank Mr. P. Y. Shieh and Ms. M. LaRosa for their valuable discussion and technical support.

†These authors contributed equally to this work.

References

1. G. Lippmann, C. R. Acad. Sci. **146**, 446 (1908).
2. L. Yang, M. McCornick, and N. Davies, Appl. Opt. **27**, 4529 (1988).
3. F. Okano, J. Arai, K. Mitani, and M. Okui, Proc. IEEE **94**, 490 (2006).
4. A. Stern and B. Javidi, Proc. IEEE **94**, 591 (2006).
5. R. Martinez-Cuenca, G. Saavedra, M. Martinez-Corral, and B. Javidi, Proc. IEEE **97**, 1067 (2009).
6. M. Cho, M. Daneshpanah, I. Moon, and B. Javidi, Proc. IEEE **99**, 556 (2011).
7. R. Schulein, M. Daneshpanah, and B. Javidi, Opt. Lett. **34**, 2012 (2009).
8. D. Shin, M. Cho, and B. Javidi, Opt. Lett. **35**, 3646 (2010).
9. S. Sato, Jpn. J. Appl. Phys. **18**, 1679 (1979).
10. H. W. Ren and S. T. Wu, Opt. Express **14**, 11292 (2006).
11. Y. P. Huang, L. Y. Liao, and C. W. Chen, J. Soc. Inf. Disp. **18**, 642 (2010).
12. Y. P. Huang and C. W. Chen, "Superzone Fresnel liquid crystal lens for temporal scanning auto-stereoscopic display," J. Disp. (to be published).
13. Y. Liu, H. W. Ren, S. Xu, Y. Chen, L. Rao, T. Ishinabe, and S. T. Wu, J. Disp. Technol. **7**, 674 (2011).
14. A. F. Namov, G. D. Love, M. Y. Loktev, and F. L. Vladimirov, Opt. Express **4**, 344 (1999).
15. C. W. Chen, Y. P. Huang, Y. C. Chang, P. H. Wang, P. C. Chen, and C. H. Tsai, Proc. SPIE **8384**, 83840W (2012).
16. Y. Li, Y. Liu, Q. Li, and S. T. Wu, Appl. Opt. **51**, 2568 (2012).
17. N. Kanopoulos, N. Vasanthavada, and R. L. Baker, IEEE J. Solid-State Circuits **23**, 358 (1988).
18. T. A. Clarke and J. F. Fryer, Photogramm. Rec. **16**, 51 (1998).